THE ROYAL SOCIETY

Intersonic crack growth on an interface

By H. H. Yu† and Z. Suo

Department of Mechanical and Aerospace Engineering and Princeton Materials Institute, Princeton University, Princeton, NJ 08544, USA

Received 19 October 1998; accepted 26 April 1999

Evidence has accumulated recently that a crack can propagate on an interface between dissimilar solids at speeds between the smallest and the largest sonic speeds of the constituent solids. Such an intersonic crack has posed several challenges to the existing theory. Assuming that the crack tip is a structureless point, and the solids are linearly elastic all the way to the crack tip, the theory shows that the stress field is singular not only at the crack tip, but also along the shock front. Furthermore, the singularity exponents differ from one half, so that the energy release rate is either zero or infinite. The relation of this theory to the experimental observations has been obscure. Specifically, it is unclear what crack speeds are forbidden by the theory. In this paper, we first introduce a unified method to analyse the crack tip field. The crack can be static, subsonic or intersonic; and the two constituent solids can be isotropic or anisotropic. To address the problem of forbidden crack speeds, we extend a cohesive zone model to intersonic cracks. In this model, the crack tip is no longer a structureless point; rather, a distributed stress represents bonding or friction. The model removes both the singular crack tip and the singular shock front. The length of the cohesive zone also characterizes the thickness of the shock front. This length depends on the crack speed. A crack speed is forbidden if it results in a negative cohesive zone length. The predictions of the model are discussed in the light of the experimental observations.

Keywords: dynamic fracture; elasticity; cohesive zone model; interface; intersonic crack; anisotropy

1. Introduction

Its relevance to composites aside, interfacial debonding provides a unique opportunity to study the fundamentals of fast cracks. The literature on a fast crack running in a homogeneous solid has been reviewed by, for example, Dmowska & Rice (1986) and Freund (1990). Under remotely applied loads, energy has to flow, via sonic waves in the solid, to a crack tip to break atomic bonds. The theory predicts that the crack can propagate at any speed below the Rayleigh wave speed of the solid. The experimentally observed tensile crack speeds, however, are often lower than half of the Rayleigh wave speed. A traditional explanation for this discrepancy invokes a common experience that, even in glass, a fast crack does not run on a plane, but creates rough surfaces (see Gao (1993) for a review). In an experiment with two

† Present address: Division of Applied Sciences and Engineering, Harvard University, Cambridge, MA 02138, USA.

Table 1. *Properties of a Plexiglas and a steel*

	ρ (kg m^{-3})	μ (GPa)	ν	c_{R} (m s^{-1})	c_{l} (m s^{-1})	c_{s} (m s^{-1})
Plexiglas	1190	2.1	0.35	1243	2330	1330
steel	7833	80	0.30	2960	5979	3196

weakly joined *identical solids*, where the weak interface confines the crack to the plane, an interfacial crack indeed approaches the Rayleigh wave speed (Washabaugh & Knauss 1994).

Early work on fast debonding of *dissimilar solids* was mainly theoretical (see, for example, Willis 1971; Wu 1991; Yang *et al*. 1991). More recent work has been largely stimulated by the experiments of Rosakis and co-workers on polymer–metal interfaces (Liu *et al*. 1993; Lambros & Rosakis 1995*a–c*; Singh *et al*. 1997). Table 1 lists the Rayleigh, the shear and the longitudinal wave speeds, $c_{\mathrm{R}}, c_{\mathrm{s}}, c_{\mathrm{l}}$, in one pair of the solids used in these experiments. The wave speeds in the steel are about three times the corresponding speeds in Plexiglas. In either solid, c_{R} is *ca.* 5% lower than c_{s}, and c_{l} is about twice that of c_{s}. In their experiments, the polymer was well bonded to the metal: the interface was about as tough as the polymer itself. A long crack was cut on the interface before loading. The specimen was then hit by a projectile launched using a gas gun, and the crack ran on the interface. Crack speeds between the shear and the longitudinal wave speeds of the polymer were recorded.

For such an intersonic crack, the stress field is governed by a mixture of elliptic and hyperbolic differential equations. Yu & Yang (1994, 1995) solved the asymptotic field around an intersonic crack on an interface between dissimilar isotropic solids. Liu *et al*. (1995) solved the case of an elastic isotropic solid bonded with a rigid solid, a system taken to approximate the polymer–metal pairs used in the above experiments. The stress field is singular not only at the crack tip, but also along the shock front in the polymer. The shock front with intense stress has been observed experimentally (Singh *et al*. 1997). The singularity exponents for the intersonic cracks differ from one half except for special crack speeds. Either infinite or vanishing energy release rate is predicted. These predictions resemble those of an earlier solution of an intersonic crack in a homogeneous isotropic solid (Freund 1990). The implications of these predictions have so far remained obscure.

The first objective of this paper is to introduce a unified method to analyse the crack tip field. Stroh (1962) showed that any two-dimensional elastic field generated by sources moving at a constant speed can be represented by six functions of the coordinates moving at the source speed. When the sources are static or subsonic, each of the six functions is a function of a complex variable. Using the Stroh representation and complex variable methods, Suo (1990) and Yang *et al*. (1991) solved the field around a crack tip on an interface between dissimilar anisotropic solids. When the source speed is intersonic, however, some of the six Stroh functions are real valued and no longer analytic. Thus, the complex variable methods cannot be applied directly. In previous works (Yu & Yang 1995; Liu *et al*. 1995), a mixture of real and complex-valued functions were used. The structure of the resulting solution is difficult to grasp. In this paper, for each real Stroh function we introduce a new analytic function whose real part equals the real function on the interface. We show that the methods developed by Suo (1990) and Yang *et al*. (1991) still apply. The advantage of this

new treatment is that it applies regardless of how large the crack speed is (static, subsonic or intersonic), or how many displacement-like quantities are involved (one for antiplane, two for inplane, three for coupled inplane and antiplane and four for piezoelectric field).

The second, perhaps conceptually more important, objective of this paper is to look for qualitative features of the theory that may be significant for crack speed selection. The existing theory has idealized the crack tip as a Euclidean point with no internal structure: linear elasticity holds all the way to the crack tip, and no bond rupture process is prescribed. It is this idealization that causes the singularity at the crack tip and the shock front. We extend the Barrenblatt (1962) cohesive zone model to intersonic cracks. In this model, a distributed stress represents the bonding or friction, removing the singularity at the crack tip. For an intersonic crack, the model also removes the singularity along the shock front. We show that this model places restrictions on the allowable crack speeds.

The paper is organized as follows. Section 2 briefly reviews the Stroh functions that represent two-dimensional elastic fields generated by steadily moving sources, and the Mach construction when the source speed exceeds a sonic speed of the solid. Section 3 represents the boundary values of traction and displacement in terms of three functions with a single complex variable. Section 4 uses this representation, together with analytic continuation, to determine the stress field around a crack running on an interface between dissimilar anisotropic solids. These general solutions are specialized to isotropic solids in § 5. Section 6 integrates the above results to solve the cohesive zone model for intersonic cracks, and discusses its experimental implications.

2. Field caused by steadily moving sources

Let (x_1, x_2, x_3) be coordinates fixed relative to a solid. In the solid, the stresses σ_{ij} relate to the displacement gradients $\partial u_k/\partial x_l$ by Hooke's law:

$$\sigma_{ij} = C_{ijkl}\partial u_k/\partial x_l. \tag{2.1}$$

The convention of summing over a repeated latin subscript is used. The elastic moduli, C_{ijkl}, satisfy the usual symmetry relations and positive-definite condition. In terms of the displacement field, the momentum balance equations are

$$C_{ijkl}\partial^2 u_k/\partial x_l \partial x_j = \rho \partial^2 u_i/\partial t^2, \tag{2.2}$$

where ρ is the mass density. These partial differential equations govern the time-dependent displacement field.

This paper considers two solids joined by a plane interface. The elastic moduli and mass density are uniform in either solid, but different from one solid to the other. On the interface there is a crack, whose front is a curve, moving at non-uniform speed. Focus on one point on the crack front. Let x_3 be tangent to the front at this point, x_1 be the crack propagation direction and v be the instantaneous crack speed at the point. We look for a singular stress field around the point. As noted in Dmowska & Rice (1986), all terms involving $\partial/\partial x_3$ can be deleted from (2.2) on grounds that they are either bounded or one order less singular than terms involving $\partial/\partial x_1$ and $\partial/\partial x_2$. On similar grounds, the acceleration $\partial^2 u_i/\partial t^2$ in (2.2) can be replaced by $v^2\partial^2 u_i/\partial x^2$, where x is a coordinate moving with the crack at that

point. Consequently, the singular field near the point moving at an instantaneous velocity v is the same as a straight crack front moving at a steady velocity v. We will focus on this two-dimensional steady-state field. This type of field was systematically studied by Stroh (1962), whose formalism is summarized as follows.

(*a*) *Stroh representation*

A body is in a state of stress independent of the coordinate x_3, and the source of stress is moving through the body at a constant speed v in the x_1 direction. Let (x, y) be a coordinate system moving at the source speed, relating to the fixed coordinates as

$$x = x_1 - vt, \qquad y = x_2. \tag{2.3}$$

To an observer moving at the same speed with this coordinate system, the steady-state field is time independent. That is, the displacements are functions of (x, y).

Consider a specific steady-state displacement field,

$$u_i = A_i f(x + py), \tag{2.4}$$

where A_1, A_2, A_3 and p are constants, and $f(\cdot)$ is a twice-differentiable, but otherwise arbitrary, one-variable function. The displacement field (2.4) will satisfy the equations of motion (2.2) provided

$$(C_{i1k1} - \rho v^2 \delta_{ik} + pC_{i1k2} + pC_{i2k1} + p^2 C_{i2k2})A_k = 0. \tag{2.5}$$

This is a set of linear algebraic equations for A_k. To represent a non-trivial displacement field, A_k cannot be all zero. Consequently, the determinant of (2.5) must vanish, which leads to a polynomial equation of degree six in p. Denote the six roots by p_α, labelling $\alpha = \pm 1, \pm 2, \pm 3$ so that, if complex roots occur, $p_{+\alpha}, p_{-\alpha}$ are complex conjugates, and giving the positive α to the root with positive imaginary part. The labelling for real roots will be specified later. Following Stroh, we will only consider the case that the p_α are all distinct; equal roots may be regarded as the limiting case of distinct roots. For each p_α, equations (2.5) determine a column $A_{k\alpha}$ up to a scaling factor. Make $A_{k\alpha}$ real when p_α is real, and $A_{k\alpha}, A_{k,-\alpha}$ complex conjugates when p_α is complex.

For any six arbitrary (twice-differentiable) functions $f_\alpha(\cdot)$, the linear combination

$$u_i = \sum_{\alpha=\pm 1}^{\pm 3} A_{i\alpha} f_\alpha(z_\alpha) \tag{2.6}$$

satisfies the governing equation (2.2). Here $z_\alpha = x + p_\alpha y$. Summation over a Greek suffix will always be indicated explicitly. Any steady-state solution to (2.2) can be represented in this form; the six Stroh functions f_α are to be determined by boundary conditions. Make f_α real when p_α is real, and $f_\alpha, f_{-\alpha}$ complex conjugate when p_α is complex, so that the displacements will always be real valued.

Substituting (2.6) into (2.1), one expresses the stresses in terms of the Stroh functions:

$$\sigma_{i2} = \sum_{\alpha=\pm1}^{\pm3} L_{i\alpha} f'_\alpha(z_\alpha), \tag{2.7}$$

$$\sigma_{i1} = -\sum_{\alpha=\pm1}^{\pm3} (L_{i\alpha} p_\alpha - \rho v^2 A_{i\alpha}) f'_\alpha(z_\alpha), \tag{2.8}$$

with

$$L_{i\alpha} = (C_{i2k1} + p_\alpha C_{i2k2}) A_{k\alpha}. \tag{2.9}$$

We use primes to indicate the differentiation of any one-variable function.

Equations (2.6)–(2.9) hold for any steady source speed whether greater or less than the sonic speeds of the solid. When $v = 0$, all the p_α are complex. When v is sufficiently large, all the p_α are real. There are three critical speeds, $V_3 \leqslant V_2 \leqslant V_1$. When v passes V_α, a pair of roots $p_{\pm\alpha}$ changes from complex to real. If then $v < V_\alpha$, the roots $p_{\pm\alpha}$ are complex, and the functions $f_{\pm\alpha}$ are complex analytic functions. If $v > V_\alpha$, the two roots $p_{\pm\alpha}$ are real, and the equations, $x + p_{\pm\alpha} y = \text{const.}$, are the characteristic lines along which the real functions $f_{\pm\alpha}$ have constant values.

(*b*) *Mach construction*

In an infinite anisotropic elastic solid, in each direction three types of plane waves can travel; they differ by their deformation states and speeds. Consider the stress field generated by a line source (i.e. a line perpendicular to the (x_1, x_2)-plane). First imagine that a stationary source at the origin O emits a single pulse at time $t = 0$, the pulse travels in all directions in the (x_1, x_2)-plane, and at $t = 1$ the pulse arrives at positions on three curves, known as the wavefronts. The intersections of these curves with the x_1-axis are the three critical speeds V_α. Label the three types of waves correspondingly as $3, 2, 1$. Next imagine a source moving at a constant velocity v along the x_1-axis. At $t = 0$ the source is at the origin O and emits a pulse. At $t = 1$ the source reaches point P, where the length OP equals v. If $v < V_3$, the source is subsonic; if $v > V_1$, the source is supersonic; otherwise, the source is intersonic. In an isotropic solid, the critical speeds, $V_3 = V_2 = c_\mathrm{s}$, and $V_1 = c_\mathrm{l}$, are independent of the running direction of the source. By contrast, in an anisotropic solid, the three critical speeds are generally distinct, and depend on the running direction of the source relative to the orientation of the solid.

The Mach construction used in aerodynamics will be essential for the analysis of intersonic cracks. Now consider a line source moving along the x_1-axis at speed v. The source emits one pulse at $t = 0$, and another pulse at $t = 1$. Figure 1 illustrates the positions of the two pulses at some later time, say $t = 3$, carried by one of the three types of sonic waves. The critical speed associated with this type of wave is V_α. At $t = 3$, the pulse emitted at $t = 0$ reaches the larger curve in figure 1, and the pulse emitted at $t = 1$ reaches the smaller curve. The dots on the x_1-axis indicate the locations of the source at various times. The current location of the source is point 3. When $v < V_\alpha$, the source is inside all the wavefronts it emitted before. When $v = V_\alpha$, all the wavefronts are tangent to one another at the source point. When $v > V_\alpha$, the

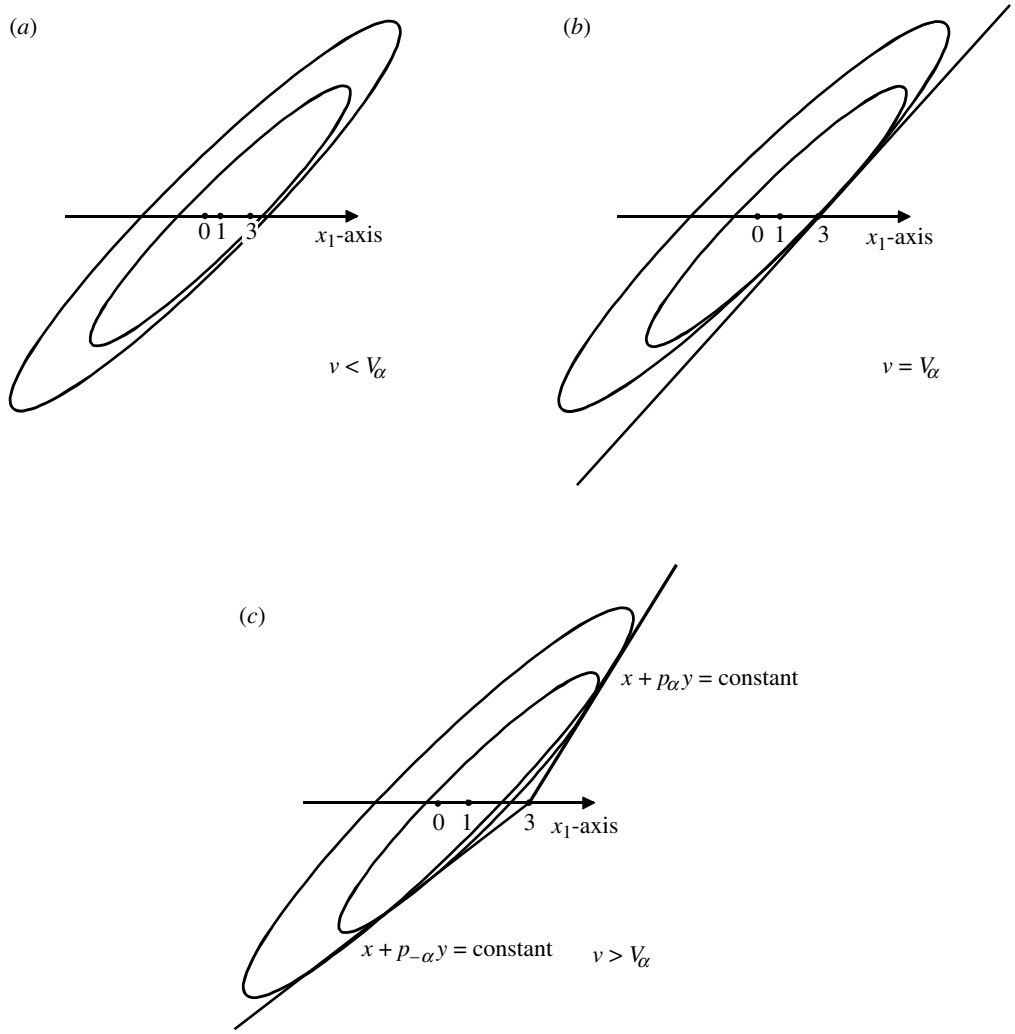

Figure 1. A source moving at velocity v emits a pulse at $t = 0$ and another pulse at $t = 1$. The positions of the two pulses at $t = 3$ are shown. V_α is a critical velocity. Three cases are considered: $v < V_\alpha$, $v = V_\alpha$ and $v > V_\alpha$.

source is outside all the wavefronts it emitted before. In the moving coordinate (x, y), the field generated by a steady source is confined between the two characteristic lines, $x + p_{+\alpha} = \text{const.}$ and $x + p_{-\alpha} y = \text{const.}$ The two lines are known as the Mach lines, and the space between the lines is the Mach wedge.

In an isotropic solid, the wavefronts due to a line source are circular, so that the Mach wedge is symmetric about the x_1-axis, and $p_{+\alpha} = -p_{-\alpha}$. We give the positive α to the positive p_α. Both Mach lines lag behind the source. By contrast, in an anisotropic solid, the Mach wedge can be asymmetric with respect to the x_1-axis, and the slope of the two Mach lines may even have the same sign, in which case, as shown in figure 1, a Mach line may extend ahead of the source (i.e. some region ahead

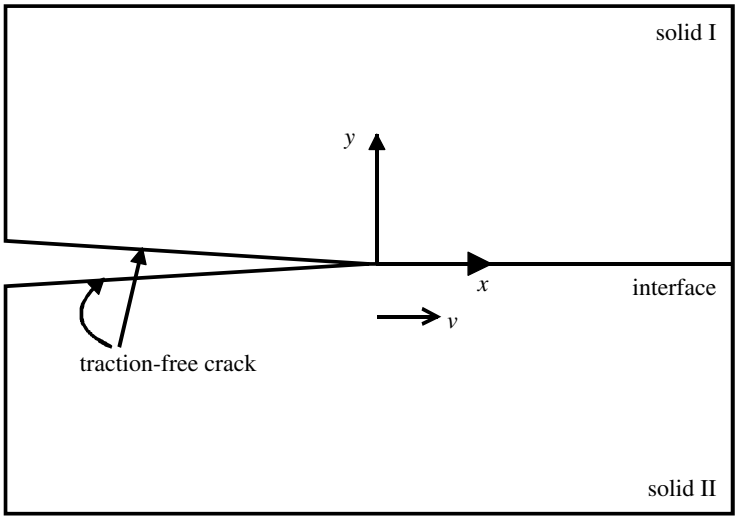

Figure 2. A crack on the interface between two semi-infinite solids, I and II.

of the source can sense the pulses emitted by the source). When $v = V_\alpha$, the two characteristic lines have the same slope and $p_{+\alpha} = p_{-\alpha}$. When $v > V_\alpha$, $p_\alpha \neq p_{-\alpha}$, we label α such that $p_\alpha > p_{-\alpha}$. Thus, when the source moves in the positive x_1-direction, p_α corresponds to the Mach line in the upper half-plane, and $p_{-\alpha}$ to the Mach line in the lower half-plane.

3. Boundary values expressed in terms of analytic functions

Figure 2 illustrates the problem to be analysed. Two semi-infinite solids, I and II, occupy the upper and lower half-planes, respectively. The crack tip moves at a constant speed v. The travelling coordinate (x, y) is centred at the crack tip, which is taken to be a mathematical point for the time being. The loads are applied remotely, the crack faces are traction-free and the displacements and tractions are continuous across the bonded interface. This section expresses the values of the displacements and tractions along the x-axis. We consider subsonic cracks and intersonic cracks in turn.

(*a*) *Subsonic*

When the crack speed is below the critical speed V_3 of both solids, all the p_α are complex. Because $(p_\alpha, p_{-\alpha})$, $(A_{k\alpha}, A_{k,-\alpha})$ and $(f_\alpha, f_{-\alpha})$ are complex-conjugate, we can rewrite (2.6) and (2.7) as

$$\begin{pmatrix} u_1 \\ u_2 \\ u_3 \end{pmatrix} = 2\,\mathrm{Re}\left\{ \begin{bmatrix} A_{11} & A_{12} & A_{13} \\ A_{21} & A_{22} & A_{23} \\ A_{31} & A_{32} & A_{33} \end{bmatrix} \begin{bmatrix} f_1(z_1) \\ f_2(z_2) \\ f_3(z_3) \end{bmatrix} \right\}, \tag{3.1}$$

$$\begin{pmatrix} \sigma_{12} \\ \sigma_{22} \\ \sigma_{32} \end{pmatrix} = 2\,\mathrm{Re}\left\{ \begin{bmatrix} L_{11} & L_{12} & L_{13} \\ L_{21} & L_{22} & L_{23} \\ L_{31} & L_{32} & L_{33} \end{bmatrix} \begin{bmatrix} f_1'(z_1) \\ f_2'(z_2) \\ f_3'(z_3) \end{bmatrix} \right\}, \tag{3.2}$$

where Re$\{\cdot\}$ denotes the real part of a complex-valued quantity. When clarity demands, a roman suffix I and II will be attached to a quantity to indicate either solid. The boundary conditions do not involve the stresses σ_{i1}, which will not be listed.

Following Suo (1990), define a function vector

$$\boldsymbol{f}(\zeta) = (f_1(\zeta), f_2(\zeta), f_3(\zeta))^{\mathrm{T}}. \tag{3.3}$$

The components are the three Stroh functions, but with a single variable $\zeta = x + \mathrm{i}y$, where $\mathrm{i} = \sqrt{-1}$. Denote the displacement vector and its derivative on the x-axis by $\boldsymbol{u}(x)$ and $\boldsymbol{u}'(x)$, and the traction vector on the x-axis by $\boldsymbol{t}(x) = \{\sigma_{2i}(x, 0)\}$. When $y = 0, \zeta, z_1, z_2, z_3$ all equal x. According to (3.1) and (3.2), we express the two vectors in terms of the boundary values of the function vector:

$$\boldsymbol{u}'(x) = \boldsymbol{A}\boldsymbol{f}'(x) + \bar{\boldsymbol{A}}\bar{\boldsymbol{f}}'(x), \tag{3.4}$$

$$\boldsymbol{t}(x) = \boldsymbol{L}\boldsymbol{f}'(x) + \bar{\boldsymbol{L}}\bar{\boldsymbol{f}}'(x), \tag{3.5}$$

where $\boldsymbol{A}$ and $\boldsymbol{L}$ are the 3×3 matrices in (3.1) and (3.2), and the conventional matrix multiplication is used.

In § 4, (3.4) and (3.5) will be used to solve for $\boldsymbol{f}(\zeta)$. Once $\boldsymbol{f}(\zeta)$ is solved, replace ζ with z_1, z_2 and z_3 for each Stroh function. If function vector $\boldsymbol{f}(\zeta)$ satisfies all the boundary conditions on the x-axis, f_1, f_2, f_3 obtained in this way also satisfy the boundary conditions. The three Stroh functions give the full field according to (3.1) and (3.2).

(*b*) *Intersonic,* $V_3^{\mathrm{I}} < v < V_2^{\mathrm{I}}$

We next show that representations similar to (3.4) and (3.5) can be obtained even for intersonic cracks. When a crack propagates in a *homogeneous solid* at a speed v surpassing V_3 but below the other two critical speeds, functions $f_3(z_3)$ and $f_{-3}(z_{-3})$ are real valued. The wave types 1 and 2 carry energy from the external load to the crack surfaces. The wave type 3 can only carry energy away from the crack surfaces. All three types of waves superpose such that the crack surfaces are traction-free. The entire crack acts as an array of line sources, all travelling at the same speed v. A line source at position $x = a$ contributes a field confined in one Mach wedge between two lines $x + p_3 y = a$ and $x + p_{-3} y = a$. The total effect of the crack is the superposition of all the wedge fields. This total effect is equivalent to selecting $f_3 \neq 0$ and $f_{-3} = 0$ for the upper plane, and $f_3 = 0$ and $f_{-3} \neq 0$ for the lower plane. Because there is no source ahead of the crack tip, $f_{\pm 3}(x) = 0$ when $x > 0$.

By contrast, when a crack propagates along a *bimaterial interface*, both the crack and the bonded interface act as sources. For the case where the crack speed only exceeds one critical speed of solid I, $v > V_3^{\mathrm{I}}$, wave type 3 in solid I can only carry energy away from the x-axis in solid I, so that $f_{-3} \equiv 0$. In general, $f_{+3} \neq 0$ both ahead and behind the crack tip. In the upper half-plane, (2.6) and (2.7) become

$$\begin{pmatrix} u_1 \\ u_2 \\ u_3 \end{pmatrix} = 2\,\mathrm{Re}\left\{ \begin{bmatrix} A_{11} & A_{12} \\ A_{21} & A_{22} \\ A_{31} & A_{32} \end{bmatrix} \begin{bmatrix} f_1(z_1) \\ f_2(z_2) \end{bmatrix} \right\} + \begin{bmatrix} A_{13} \\ A_{23} \\ A_{33} \end{bmatrix} f_3(z_3), \tag{3.6}$$

$$\begin{pmatrix} \sigma_{12} \\ \sigma_{22} \\ \sigma_{32} \end{pmatrix} = 2\,\mathrm{Re}\left\{ \begin{bmatrix} L_{11} & L_{12} \\ L_{21} & L_{22} \\ L_{31} & L_{32} \end{bmatrix} \begin{bmatrix} f_1'(z_1) \\ f_2'(z_2) \end{bmatrix} \right\} + \begin{bmatrix} L_{13} \\ L_{23} \\ L_{33} \end{bmatrix} f_3'(z_3). \tag{3.7}$$

Here A_{i3}, L_{i3}, z_3 and f_3 are real, and f_1, f_2 remain as analytic functions in the upper half-plane.

The real-valued function $f_3(x + p_3 y)$ is not analytic. Introduce a complex-valued function $F_3(\zeta)$, which is analytic in the upper half-plane and satisfies

$$f_3(x) = 2\,\mathrm{Re}(F_3^+(x)) \tag{3.8}$$

along the x-axis. The superscript '+' indicates the limiting value of the analytic function approaching from the upper half-plane to a point on the x-axis. The existence of such an analytic function was proved in Muskhelishvili (1953).

Now define an analytic function vector for solid I as

$$\boldsymbol{f}_{\mathrm{I}}(\zeta) = (f_1(\zeta), f_2(\zeta), F_3(\zeta))^{\mathrm{T}}. \tag{3.9}$$

The first two components are the Stroh functions, and the third is the newly defined analytic function. Again, when $y = 0$, ζ, z_1, z_2, z_3 all equal x. According to (3.6) and (3.7), we express the displacements and tractions on the x-axis in the same form as (3.4) and (3.5). Now the last columns of the two matrices $\boldsymbol{A}$ and $\boldsymbol{L}$ are the real numbers $\{A_{i3}\}$ and $\{L_{i3}\}$. Once $\boldsymbol{f}_{\mathrm{I}}(\zeta)$ is solved, as will be done in § 4, replace ζ by z_1, z_2 in $f_1(\zeta)$ and $f_2(\zeta)$; obtain $f_3(x)$ by the real part of $F_3(\zeta)$ when $\zeta \to x + 0 \cdot \mathrm{i}$ and then replace x in $f_3(x)$ by $z_3 = x + p_3 y$. The Stroh functions obtained this way give the full field according to (3.6) and (3.7).

(*c*) *Intersonic, $V_3^{\mathrm{II}} < v < V_2^{\mathrm{II}}$; and other crack speeds*

If the crack speed just exceeds the critical speed V_3 of solid II, $f_{+3}(x) = 0$, but in general $f_{-3}(x) \neq 0$ along the entire x-axis. In the lower half-plane, (2.6) and (2.7) become

$$\begin{pmatrix} u_1 \\ u_2 \\ u_3 \end{pmatrix} = 2\,\mathrm{Re}\left\{ \begin{bmatrix} A_{11} & A_{12} \\ A_{21} & A_{22} \\ A_{31} & A_{32} \end{bmatrix} \begin{bmatrix} f_1(z_1) \\ f_2(z_2) \end{bmatrix} \right\} + \begin{bmatrix} A_{1,-3} \\ A_{2,-3} \\ A_{3,-3} \end{bmatrix} f_{-3}(z_{-3}), \tag{3.10}$$

$$\begin{pmatrix} \sigma_{12} \\ \sigma_{22} \\ \sigma_{32} \end{pmatrix} = 2\,\mathrm{Re}\left\{ \begin{bmatrix} L_{11} & L_{12} \\ L_{21} & L_{22} \\ L_{31} & L_{32} \end{bmatrix} \begin{bmatrix} f_1'(z_1) \\ f_2'(z_2) \end{bmatrix} \right\} + \begin{bmatrix} L_{1,-3} \\ L_{2,-3} \\ L_{3,-3} \end{bmatrix} f_{-3}'(z_{-3}). \tag{3.11}$$

Again introduce a complex-valued function $F_{-3}(\zeta)$, which is analytic in the lower half-plane and satisfies $f_{-3}(x) = 2\,\mathrm{Re}(F_{-3}^-(x))$. Here the superscript '−' indicates the limiting value of the analytic functions approaching from the lower half-plane to a point on the x-axis. We define a vector function

$$\boldsymbol{f}_{\mathrm{II}}(\zeta) = (f_1(\zeta), f_2(\zeta), F_{-3}(\zeta))^{\mathrm{T}}. \tag{3.12}$$

According to (3.10) and (3.11), we can write the displacement and stress vector on the x-axis in the same form as (3.4) and (3.5). The last columns of the two matrices $\boldsymbol{A}$, $\boldsymbol{L}$ are the real numbers $\{A_{i,-3}\}$ and $\{L_{i,-3}\}$.

The treatment for other crack speeds is similar. In particular, when $v > V_1^{\mathrm{I}}$, all six roots $p_{\pm\alpha}$ are real. We can still define three analytic functions whose real parts on the x-axis equal the values of f_1, f_2, f_3. The displacement and traction vectors on the x-axis can still be represented by the three analytic functions as (3.4) and (3.5). This treatment is useful when the crack speed exceeds the three critical speeds of solid I but is still below some of the critical speeds of solid II.

4. Crack tip field

We will assume small-scale yielding and small-scale contact near the crack tip. This section concentrates on the field outside the small-scale nonlinear zone. In § 6, we will study the effect of the nonlinear zone.

(a) *Important matrices*

Several matrices to be used below are briefly discussed here. As stated in § 2, each column $\{A_{i\alpha}\}$ is determined up to a complex- or real-valued scalar. Once this scalar is fixed, $\{A_{i\alpha}\}$ is fixed and, following (2.9), $\{L_{i\alpha}\}$ is also fixed. Consequently, the 3×3 matrices $\boldsymbol{A}$ and $\boldsymbol{L}$ assembled in § 3 for various source speeds are determined up to three scalars.

Define another 3×3 matrix, $\boldsymbol{B} = \mathrm{i}\boldsymbol{A}\boldsymbol{L}^{-1}$. The matrix is fully determined by the elastic moduli and source speed v with no arbitrary scalars, and has the unit of inverse elastic modulus. The matrix $\boldsymbol{B}$ is the inverse of the surface impedance matrix used in the literature of surface waves (see, for example, Barnett & Lothe 1985). That literature has been mainly concerned with subsonic source speed, where $\boldsymbol{B}$ is Hermitian, namely $\boldsymbol{B}^{\mathrm{T}} = \bar{\boldsymbol{B}}$. When $v > V_3$, however, our calculation shows that $\boldsymbol{B}$ is no longer Hermitian. As will be clear later, this fact has a profound effect on intersonic crack tip field. The appendix relates $\boldsymbol{B}$ to the two real matrices introduced in Yu & Yang (1995).

Denote $\boldsymbol{B}_{\mathrm{I}}$ and $\boldsymbol{B}_{\mathrm{II}}$ as the above-defined matrix for the two solids, respectively. Define a bimaterial matrix $\boldsymbol{H} = \boldsymbol{B}_{\mathrm{I}} + \bar{\boldsymbol{B}}_{\mathrm{II}}$. Separate the real and imaginary parts as $\boldsymbol{H} = \boldsymbol{M} + \mathrm{i}\boldsymbol{N}$. For a subsonic crack, because both $\boldsymbol{B}_{\mathrm{I}}$ and $\boldsymbol{B}_{\mathrm{II}}$ are Hermitian, $\boldsymbol{H}$ is Hermitian, $\boldsymbol{M}$ is symmetric and $\boldsymbol{N}$ is antisymmetric. These properties are lost for intersonic cracks.

(b) *Analytic continuation*

For any crack speed (static, subsonic or intersonic), we have defined analytic function vectors $\boldsymbol{f}_{\mathrm{I}}(\zeta)$ and $\boldsymbol{f}_{\mathrm{II}}(\zeta)$ for the two solids, and used them to represent the displacement and traction vectors on the x-axis, (3.4) and (3.5). Here we apply various boundary conditions to solve for $\boldsymbol{f}_{\mathrm{I}}(\zeta)$ and $\boldsymbol{f}_{\mathrm{II}}(\zeta)$. Because we have written the boundary conditions into the same form for any crack speed, our solution procedure here will follow closely that of Suo (1990) for a static crack, and of Yang *et al*. (1991) for a subsonic crack, on an interface between dissimilar anisotropic solids. The procedure is a generalization of that of Rice (1988) for a static crack on an interface between dissimilar isotropic solids.

The traction $\boldsymbol{t}(x)$ is continuous across the whole x-axis, both the bonded and the cracked portions. According to (3.5), this continuity is written as

$$\boldsymbol{L}_{\mathrm{I}}\boldsymbol{f}'_{\mathrm{I}}(x) + \bar{\boldsymbol{L}}_{\mathrm{I}}\bar{\boldsymbol{f}}'_{\mathrm{I}}(x) = \boldsymbol{L}_{\mathrm{II}}\boldsymbol{f}'_{\mathrm{II}}(x) + \bar{\boldsymbol{L}}_{\mathrm{II}}\bar{\boldsymbol{f}}'_{\mathrm{II}}(x). \tag{4.1}$$

Observe that $\boldsymbol{f}'_{\mathrm{I}}(\zeta)$ and $\bar{\boldsymbol{f}}'_{\mathrm{II}}(\zeta)$ are analytic in the upper half-plane, and $\bar{\boldsymbol{f}}'_{\mathrm{I}}(\zeta)$ and $\boldsymbol{f}'_{\mathrm{II}}(\zeta)$ are analytic in the lower half-plane. Analytic continuation (4.1) requires that

$$\boldsymbol{L}_{\mathrm{I}}\boldsymbol{f}'_{\mathrm{I}}(\zeta) - \bar{\boldsymbol{L}}_{\mathrm{II}}\bar{\boldsymbol{f}}'_{\mathrm{II}}(\zeta) = \boldsymbol{g}(\zeta), \quad \zeta \in \mathrm{I}, \tag{4.2a}$$

$$\boldsymbol{L}_{\mathrm{II}}\boldsymbol{f}'_{\mathrm{II}}(\zeta) - \bar{\boldsymbol{L}}_{\mathrm{I}}\bar{\boldsymbol{f}}'_{\mathrm{I}}(\zeta) = \boldsymbol{g}(\zeta), \quad \zeta \in \mathrm{II}. \tag{4.2b}$$

Here $\boldsymbol{g}(\zeta)$ is an analytic function in the whole plane excluding the crack tip, $\zeta = 0$. A comparison of (4.2 *a*) and (4.2 *b*) shows that $\bar{\boldsymbol{g}}(\zeta) = -\boldsymbol{g}(\zeta)$.

The displacement $\boldsymbol{u}(x)$ is continuous across the bonded interface, so is the derivative $\boldsymbol{u}'(x)$. According to (3.4), this continuity is written as

$$\boldsymbol{A}_{\mathrm{I}}\boldsymbol{f}_{\mathrm{I}}'(x) + \bar{\boldsymbol{A}}_{\mathrm{I}}\bar{\boldsymbol{f}}_{\mathrm{I}}'(x) = \boldsymbol{A}_{\mathrm{II}}\boldsymbol{f}_{\mathrm{II}}'(x) + \bar{\boldsymbol{A}}_{\mathrm{II}}\bar{\boldsymbol{f}}_{\mathrm{II}}'(x), \quad 0 < x < +\infty. \tag{4.3}$$

Using (4.2) to eliminate $\boldsymbol{f}_{\mathrm{I}}'$ and $\boldsymbol{f}_{\mathrm{II}}'$ from (4.3), we obtain that

$$\boldsymbol{L}_{\mathrm{I}}\boldsymbol{f}_{\mathrm{I}}'(x) = \boldsymbol{H}^{-1}[\bar{\boldsymbol{H}}\boldsymbol{L}_{\mathrm{II}}\boldsymbol{f}_{\mathrm{II}}'(x) - (\bar{\boldsymbol{B}}_{\mathrm{I}} - \bar{\boldsymbol{B}}_{\mathrm{II}})\boldsymbol{g}(x)], \quad 0 < x < +\infty. \tag{4.4}$$

Because $\boldsymbol{f}_{\mathrm{I}}'(\zeta)$ is analytic in the upper half-plane and $\boldsymbol{f}_{\mathrm{II}}'(\zeta)$ is analytic in the lower half-plane, the continuity (4.4) requires that there exists a function vector $\boldsymbol{h}(\zeta)$, analytic in the entire plane excluding the crack $-\infty < x < 0$, such that

$$\boldsymbol{h}(\zeta) = \begin{cases} \boldsymbol{L}_{\mathrm{I}}\boldsymbol{f}_{\mathrm{I}}'(\zeta), & \zeta \in \mathrm{I}, \\ \boldsymbol{H}^{-1}[\bar{\boldsymbol{H}}\boldsymbol{L}_{\mathrm{II}}\boldsymbol{f}_{\mathrm{II}}'(\zeta) - (\bar{\boldsymbol{B}}_{\mathrm{I}} - \bar{\boldsymbol{B}}_{\mathrm{II}})\boldsymbol{g}(\zeta)], & \zeta \in \mathrm{II}. \end{cases} \tag{4.5}$$

Equations (4.5) can be used to express both $\boldsymbol{f}_{\mathrm{I}}'(\zeta)$ and $\boldsymbol{f}_{\mathrm{II}}'(\zeta)$ in terms of $\boldsymbol{h}(\zeta)$ and $\boldsymbol{g}(\zeta)$. These results, combined with (4.2) and (3.5), give the traction on the whole x-axis:

$$\boldsymbol{t}(x) = \boldsymbol{h}^{+}(x) + \bar{\boldsymbol{H}}^{-1}\boldsymbol{H}\boldsymbol{h}^{-}(x) - 2\bar{\boldsymbol{H}}^{-1}\,\mathrm{Re}(\boldsymbol{B}_{\mathrm{II}})\boldsymbol{g}(x). \tag{4.6}$$

Denote the displacement jump across the crack by $\boldsymbol{d}(x) = \boldsymbol{u}_{\mathrm{I}}(x) - \boldsymbol{u}_{\mathrm{II}}(x)$. A direct calculation shows that

$$\mathrm{i}\boldsymbol{d}'(x) = \boldsymbol{H}(\boldsymbol{h}^{+}(x) - \boldsymbol{h}^{-}(x)). \tag{4.7}$$

(*c*) *Riemann–Hilbert problem*

From (4.6), the traction-free condition on the crack surface becomes

$$\bar{\boldsymbol{H}}\boldsymbol{h}^{+}(x) + \boldsymbol{H}\boldsymbol{h}^{-}(x) = 2\,\mathrm{Re}(\boldsymbol{B}_{\mathrm{II}})\boldsymbol{g}(x), \quad x < 0. \tag{4.8}$$

This is a Riemann–Hilbert problem that governs $\boldsymbol{h}(\zeta)$. One can confirm that a particular solution to (4.8) is

$$\boldsymbol{h}(\zeta) = \boldsymbol{M}^{-1}\,\mathrm{Re}(\boldsymbol{B}_{\mathrm{II}})\boldsymbol{g}(\zeta). \tag{4.9 a}$$

A homogeneous solution to (4.8) is of the form

$$\boldsymbol{h}(\zeta) = \zeta^{\lambda}\boldsymbol{w}, \tag{4.9 b}$$

where $\boldsymbol{w}$ is a constant vector and λ is a constant number. The crack $-\infty < x < 0$ is the branch cut for the function ζ^{λ}. Let (r, θ) be a polar coordinate centred at the crack tip and $\zeta = r\exp(\mathrm{i}\theta)$, so that $\zeta^{\lambda} = r^{\lambda}\exp(\mathrm{i}\lambda\theta)$, where $\theta = \pm\pi$ represent the two crack surfaces. A substitution of (4.9) into the homogeneous form of (4.8) gives a generalized eigenvalue problem:

$$\boldsymbol{H}\boldsymbol{w} = -\exp(2\pi\mathrm{i}\lambda)\bar{\boldsymbol{H}}\boldsymbol{w}. \tag{4.10 a}$$

In terms of the real matrices defined in § 4*a*, the eigenvalue problem is written as

$$[\cos(\pi\lambda)\boldsymbol{M} + \sin(\pi\lambda)\boldsymbol{N}]\boldsymbol{w} = 0. \tag{4.10 b}$$

Evidently, if $(\lambda, \boldsymbol{w})$ is a set of eigenvalue and eigenvector, so are $(\bar{\lambda}, \bar{\boldsymbol{w}})$ and $(\lambda \pm 1, \boldsymbol{w})$. If we confine the real part of λ in the interval $(-1, 0]$, (4.10) has only three eigenvalues, denoted as λ_β $(\beta = 1, 2, 3)$. They can be all real, or one real and two complex conjugates. Each eigenvector $\boldsymbol{w}_\beta$ is determined up to one scalar; we normalize $\boldsymbol{w}_\beta$ such that $\bar{\boldsymbol{w}}_\beta^{\mathrm{T}} \cdot \boldsymbol{w}_\beta = 1$.

If $\boldsymbol{h}(\zeta) = \zeta^\lambda \boldsymbol{w}$ is a homogeneous solution to (4.8), then $\boldsymbol{h}\zeta = a(\zeta)\zeta^\lambda \boldsymbol{w}$ is also a homogeneous solution, provided $a(\zeta)$ is analytic in the entire plane excluding the crack tip. The general solution to (4.8) is the superposition of a particular solution and all homogeneous solutions. We write the general solution in the form

$$\boldsymbol{h}(\zeta) = \sum_{\beta=1}^{3} \frac{k_\beta(\zeta)}{1 - \exp(2\pi \mathrm{i} \lambda_\beta)} \zeta^{\lambda_\beta} \boldsymbol{w}_\beta + \boldsymbol{M}^{-1} \operatorname{Re}(\boldsymbol{B}_{\mathrm{II}}) \boldsymbol{g}(\zeta), \tag{4.11}$$

where $k_\beta(\zeta)$ are functions analytic in the entire plane excluding the crack tip.

Inserting (4.11) into (4.6), we find the traction on the bonded interface a distance r ahead of the crack tip:

$$\boldsymbol{t}(r) = \sum_{\beta=1}^{3} k_\beta(r) r^{\lambda_\beta} \boldsymbol{w}_\beta. \tag{4.12}$$

In (4.11), we have multiplied some constants to the homogeneous solution such that the expression for the traction (4.12) looks simple. Because $\boldsymbol{t}(r)$ is real valued, the three functions k_1, k_2, k_3 must be further restricted. We choose λ_3 and $\boldsymbol{w}_3$ to be real, so that $k_3(\zeta) = \bar{k}_3(\zeta)$. If λ_1 and λ_2 are real numbers, $k_1(\zeta) = \bar{k}_1(\zeta)$ and $k_2(\zeta) = \bar{k}_2(\zeta)$. If (λ_1, λ_2) are complex conjugates, $k_1(\zeta) = \bar{k}_2(\zeta)$.

Inserting the general solution (4.11) into (4.5), we obtain the vector functions in the two solids:

$$\boldsymbol{f}'_{\mathrm{I}}(\zeta) = \boldsymbol{L}_{\mathrm{I}}^{-1} \left[\sum_{\beta=1}^{3} \frac{k_\beta(\zeta)}{1 - \exp(2\pi \mathrm{i} \lambda_\beta)} \zeta^{\lambda_\beta} \boldsymbol{w}_\beta + \boldsymbol{M}^{-1} \operatorname{Re}(\boldsymbol{B}_{\mathrm{II}}) \boldsymbol{g}(\zeta) \right], \tag{4.13}$$

$$\boldsymbol{f}'_{\mathrm{II}}(\zeta) = \boldsymbol{L}_{\mathrm{II}}^{-1} \left[\sum_{\beta=1}^{3} \frac{k_\beta(\zeta)}{1 - \exp(-2\pi \mathrm{i} \lambda_\beta)} \zeta^{\lambda_\beta} \boldsymbol{w}_\beta + \boldsymbol{M}^{-1} \operatorname{Re}(\boldsymbol{B}_{\mathrm{I}}) \boldsymbol{g}(\zeta) \right]. \tag{4.14}$$

Following the procedure described in § 3, one can calculate the stress and the displacement fields in both solids.

(*d*) *Williams-type expansion*

A Williams-type expansion (Williams 1959) can be generated from (4.11)–(4.14) by writing $k_\beta(\zeta)$ and $\boldsymbol{g}(\zeta)$ as the Laurent series. As discussed in the beginning of § 2, we are looking for a singular stress field near the crack tip. Consequently, only the terms leading to a singular stress field are retained:

$$k_\beta(\zeta) = \sum_{n=-\infty}^{0} a_{\beta n} \zeta^n, \quad g_i(\zeta) = \sum_{n=-\infty}^{-1} b_{in} \zeta^n. \tag{4.15}$$

The coefficients a_{3n} and b_{in} are real and imaginary numbers, respectively. If λ_1 and λ_2 are real, so are a_{1n} and a_{2n}. If λ_1 and λ_2 are complex conjugate, so are a_{1n} and

a_{2n}. The full set of the Williams eigenvalues have the form $\lambda_\beta + n$ and n, where $-1 < \lambda_\beta < 0$ and n is an arbitrary integer.

In the above series $a_{\beta 0}$, reduce to the three conventional stress intensity factors for a static crack in a homogeneous solid. The physical significance of other terms in the series has been discussed by Rice (1988) and Hui & Ruina (1995) in the context of static cracks. We will not pursue a parallel discussion for intersonic cracks in this paper. Instead, we will focus on the $a_{\beta 0}$ terms. Denote $K_\beta = a_{\beta 0}$, $\beta = 1, 2, 3$. Associated with the $a_{\beta 0}$ terms, the traction a distance r ahead of the crack tip is given by

$$\boldsymbol{t}(r) = \sum_{\beta=1}^{3} K_\beta r^{\lambda_\beta} \boldsymbol{w}_\beta. \tag{4.16}$$

The displacement jump a distance r behind the crack tip is

$$\boldsymbol{d}(r) = \sum_{\beta=1}^{3} \frac{K_\beta r^{1+\lambda_\beta} \boldsymbol{M}\boldsymbol{w}_\beta}{(1+\lambda_\beta)\sin(-\pi\lambda_\beta)}. \tag{4.17}$$

The expressions (4.16) and (4.17) specialize to familiar forms for several well-known situations. For a static or subsonic crack in a homogeneous solid, $\lambda_1 = \lambda_2 = \lambda_3 = -\frac{1}{2}$, $\boldsymbol{w}_1 = [1, 0, 0]$, $\boldsymbol{w}_2 = [0, 1, 0]$, $\boldsymbol{w}_3 = [0, 0, 1]$, so that K_1, K_2 and K_3 are the stress intensity factors for the in-plane shear, the opening and the anti-plane shear modes. (We have removed the factor $\sqrt{2\pi}$ from the definition, because it serves no useful purpose in more general situations.)

For a static or a subsonic crack on a bimaterial interface, when the bimaterial has such a symmetry that the in-plane and the anti-plane deformation decouple, $\lambda_3 = -\frac{1}{2}$ and $\boldsymbol{w}_3 = [0, 0, 1]$ so that K_3 corresponds to the anti-plane mode; and $\lambda_1 = \bar{\lambda}_2 = -\frac{1}{2} + \mathrm{i}\varepsilon$ and $\boldsymbol{w}_1 = \bar{\boldsymbol{w}}_2 = [\gamma, \eta, 0]$, where $\varepsilon, \gamma, \eta$ are numbers determined by the eigenvalue problem (4.10), so that $K_1 = \bar{K}_2$ correspond to the coupled in-plane modes. The structure of the field has been discussed by Rice (1988) for a static crack on an interface between dissimilar isotropic solids, by Suo (1990) for a static crack on an interface between dissimilar anisotropic solids and by Yang *et al.* (1991) for a subsonic interfacial crack.

For an intersonic crack between dissimilar isotropic solids, Yu & Yang (1995) showed that λ_1 and λ_2 can be both real, or be complex conjugate; and $\mathrm{Re}(\lambda_1)$ and $\mathrm{Re}(\lambda_2)$ differ from $-\frac{1}{2}$ in general.

5. In-plane fields in bonded isotropic solids

In this section, using the method of this paper, we reproduce the results of Freund (1990), Yu & Yang (1995) and Liu *et al.* (1995) for isotropic solids. The results will be used in the next section to analyse the cohesive zone model.

For two isotropic solids joined by a plane interface, the anti-plane and the in-plane deformation decouple. We will only consider the in-plane deformation, for which the determinant of (2.5) has four roots:

$$p_{\pm 1}^2 = v^2/c_1^2 - 1, \qquad p_{\pm 2}^2 = v^2/c_s^2 - 1. \tag{5.1}$$

The longitudinal and shear wave speeds are given by

$$c_{\mathrm{l}} = \left[\frac{2(1-\nu)\mu}{(1-2\nu)\rho}\right]^{1/2}, \qquad c_{\mathrm{s}} = \left(\frac{\mu}{\rho}\right)^{1/2}, \tag{5.2}$$

where μ is the shear modulus, ν is Poisson's ratio and ρ is the mass density. It is evident from (5.1) that c_{l} and c_{s} are also the critical speeds. When the crack speed v surpasses c_{l} or c_{s}, a pair of roots changes from complex to real.

The related matrices are all 2×2, as given by

$$\boldsymbol{A} = \begin{bmatrix} 1 & -p_2 \\ p_1 & 1 \end{bmatrix}, \tag{5.3}$$

$$\boldsymbol{L} = \mu \begin{bmatrix} 2p_1 & 1-p_2^2 \\ -(1-p_2^2) & 2p_2 \end{bmatrix}, \tag{5.4}$$

$$\boldsymbol{B} = \frac{\mathrm{i}}{\mu[4p_1p_2 + (1-p_2^2)^2]} \begin{bmatrix} p_2(1+p_2^2) & p_2^2 - 1 - 2p_1p_2 \\ 2p_1p_2 + 1 - p_2^2 & p_1(1+p_2^2) \end{bmatrix}. \tag{5.5}$$

Replace p_2 with p_{-2} if $c_{\mathrm{s}} < v < c_{\mathrm{l}}$ and the solid is in the lower half-plane.

For a subsonic crack, $v < c_{\mathrm{s}}$, all roots are imaginary numbers:

$$p_1 = \mathrm{i}\sqrt{1 - v^2/c_{\mathrm{l}}^2} \equiv \mathrm{i}\alpha_{\mathrm{l}}, \qquad p_2 = \mathrm{i}\sqrt{1 - v^2/c_{\mathrm{s}}^2} \equiv \mathrm{i}\alpha_{\mathrm{s}}, \tag{5.6}$$

so that

$$\boldsymbol{B} = \frac{1}{\mu[4\alpha_{\mathrm{l}}\alpha_{\mathrm{s}} - (1+\alpha_{\mathrm{s}}^2)^2]} \begin{bmatrix} \alpha_{\mathrm{s}}(1-\alpha_{\mathrm{s}}^2) & \mathrm{i}(-2\alpha_{\mathrm{l}}\alpha_{\mathrm{s}} + 1 + \alpha_{\mathrm{s}}^2 \\ \mathrm{i}(2\alpha_{\mathrm{l}}\alpha_{\mathrm{s}} - 1 - \alpha_{\mathrm{s}}^2) & \alpha_{\mathrm{l}}(1-\alpha_{\mathrm{s}}^2) \end{bmatrix}. \tag{5.7}$$

As expected, this matrix is Hermitian.

For an intersonic crack, $c_{\mathrm{s}} < v < c_{\mathrm{l}}$, $p_{\pm 2}$ become real but $p_{\pm 1}$ are still imaginary:

$$p_1 = \mathrm{i}\alpha_{\mathrm{l}}, \qquad p_2 = \sqrt{v^2/c_{\mathrm{s}}^2 - 1} = \hat{\alpha}_{\mathrm{s}}. \tag{5.8}$$

If the crack speed is between sonic speeds of the solid I in the upper half-plane,

$$\boldsymbol{B}_{\mathrm{I}} = \frac{\mathrm{i}}{\mu(4\mathrm{i}\hat{\alpha}_{\mathrm{s}}\alpha_{\mathrm{l}} + (1-\hat{\alpha}_{\mathrm{s}}^2)^2} \begin{bmatrix} \hat{\alpha}_{\mathrm{s}}(1+\hat{\alpha}_{\mathrm{s}}^2) & \hat{\alpha}_{\mathrm{s}}^2 - 1 - 2\mathrm{i}\hat{\alpha}_{\mathrm{s}}\alpha_{\mathrm{l}} \\ -\hat{\alpha}_{\mathrm{s}}^2 + 1 + 2\mathrm{i}\hat{\alpha}_{\mathrm{s}}\alpha_{\mathrm{l}} & \mathrm{i}\alpha_{\mathrm{l}}(1+\hat{\alpha}_{\mathrm{s}}^2) \end{bmatrix}. \tag{5.9}$$

Note that $\boldsymbol{B}_{\mathrm{I}}$ is no longer Hermitian. If the crack speed is intersonic for solid II in the lower half-plane, $\boldsymbol{B}_{\mathrm{II}}$ has an expression similar to (5.9) with $\hat{\alpha}_{\mathrm{s}}$ replaced by $-\hat{\alpha}_{\mathrm{s}}$. We next list crack tip fields for two limiting cases of the relative stiffness of the two joining solids.

(*a*) *Solid I and solid II are identical*

This case was considered by Freund (1990). For a subsonic crack, $v < c_{\mathrm{s}}$, $\boldsymbol{B}_{\mathrm{I}}$ and $\boldsymbol{B}_{\mathrm{II}}$ are identical, as given by (5.7). Consequently, the matrix $\boldsymbol{H} = \boldsymbol{B}_{\mathrm{I}} + \boldsymbol{B}_{\mathrm{II}}$ is real valued:

$$\boldsymbol{H} = \frac{2(1-\alpha_{\mathrm{s}}^2)}{\mu[4\alpha_{\mathrm{l}}\alpha_{\mathrm{s}} - (1+\alpha_{\mathrm{s}}^2)^2]} \begin{bmatrix} \alpha_{\mathrm{s}} & 0 \\ 0 & \alpha_{\mathrm{l}} \end{bmatrix}. \tag{5.10}$$

The eigenvalue problem (4.10) leads to

$$\lambda_1 = \lambda_2 = -\tfrac{1}{2} \quad \text{and} \quad \boldsymbol{w}_1 = \begin{pmatrix} 1 \\ 0 \end{pmatrix}, \quad \boldsymbol{w}_2 = \begin{pmatrix} 0 \\ 1 \end{pmatrix}. \tag{5.11}$$

These are well-known results (Freund 1990). For a subsonic crack running in an isotropic homogeneous solid, the crack tip field contains the shear and the tensile modes, both being square-root singular. The tractions a distance r ahead of the crack tip are

$$\sigma_{21} = K_1 r^{-1/2}, \qquad \sigma_{22} = K_2 r^{-1/2}. \tag{5.12}$$

The displacement jumps a distance r behind the crack tip are

$$\begin{bmatrix} d_1 \\ d_2 \end{bmatrix} = \frac{4(1-\alpha_{\mathrm{s}}^2) r^{1/2}}{\mu[4\alpha_{\mathrm{l}}\alpha_{\mathrm{s}} - (1+\alpha_{\mathrm{s}}^2)^2]} \begin{bmatrix} \alpha_{\mathrm{s}} K_1 \\ \alpha_{\mathrm{l}} K_2 \end{bmatrix}. \tag{5.13}$$

For an intersonic crack, $c_{\mathrm{s}} < v < c_{\mathrm{l}}$, $\boldsymbol{B}_{\mathrm{I}}$ is given by (5.9), and $\boldsymbol{B}_{\mathrm{II}}$ is given by a similar expression with $\hat{\alpha}_{\mathrm{s}}$ replaced by $-\hat{\alpha}_{\mathrm{s}}$. Consequently,

$$\boldsymbol{H} = \frac{1+\hat{\alpha}_{\mathrm{s}}^2}{\mu(4\mathrm{i}\alpha_{\mathrm{l}}\hat{\alpha}_{\mathrm{s}} + (1-\hat{\alpha}_{\mathrm{s}}^2)^2)} \begin{bmatrix} 2\hat{\alpha}_{\mathrm{s}}\mathrm{i} & 0 \\ 0 & -2\alpha_{\mathrm{l}} \end{bmatrix}. \tag{5.14}$$

This matrix is complex valued and non-Hermitian. Its real and imaginary parts are

$$\left.\begin{aligned} \boldsymbol{M} &= \frac{2\alpha_{\mathrm{l}}(\hat{\alpha}_{\mathrm{s}}^2+1)}{[16\hat{\alpha}_{\mathrm{s}}^2\alpha_{\mathrm{l}}^2 + (\hat{\alpha}_{\mathrm{s}}^2-1)^4]\mu} \begin{bmatrix} 4\hat{\alpha}_{\mathrm{s}}^2 & 0 \\ 0 & -(\hat{\alpha}_{\mathrm{s}}^2-1)^2 \end{bmatrix}, \\ \boldsymbol{N} &= \frac{2\hat{\alpha}_{\mathrm{s}}(\hat{\alpha}_{\mathrm{s}}^2+1)}{[16\hat{\alpha}_{\mathrm{s}}^2\alpha_{\mathrm{l}}^2 + (\hat{\alpha}_{\mathrm{s}}^2-1)^4]\mu} \begin{bmatrix} (\hat{\alpha}_{\mathrm{s}}^2-1)^2 & 0 \\ 0 & 4\alpha_{\mathrm{l}}^2 \end{bmatrix}. \end{aligned}\right\} \tag{5.15}$$

The eigenvalue problem (4.10) leads to

$$\lambda_1 = -\frac{1}{\pi}\tan^{-1}\frac{4\alpha_{\mathrm{l}}\hat{\alpha}_{\mathrm{s}}}{(1-\hat{\alpha}_{\mathrm{s}}^2)^2}, \quad \boldsymbol{w}_1 = \begin{pmatrix} 1 \\ 0 \end{pmatrix}, \tag{5.16a}$$

$$\lambda_2 = \lambda_1 - \tfrac{1}{2} = -\frac{1}{\pi}\tan^{-1}\frac{(1-\hat{\alpha}_{\mathrm{s}}^2)^2}{4\alpha_{\mathrm{l}}\hat{\alpha}_{\mathrm{s}}}, \quad \boldsymbol{w}_2 = \begin{pmatrix} 0 \\ 1 \end{pmatrix}. \tag{5.16b}$$

The value of $\tan^{-1}(\cdot)$ is taken from 0 to π. The tractions a distance r ahead of the crack tip are

$$\sigma_{21} = K_1 r^{\lambda_1}, \qquad \sigma_{22} = K_2 r^{\lambda_2}. \tag{5.17}$$

The displacement jumps a distance r behind the crack tip are

$$\begin{bmatrix} d_1 \\ d_2 \end{bmatrix} = \frac{2\alpha_{\mathrm{l}}(\hat{\alpha}_{\mathrm{s}}^2+1)}{[16\hat{\alpha}_{\mathrm{s}}^2\alpha_{\mathrm{l}}^2 + (\hat{\alpha}_{\mathrm{s}}^2-1)^4]\mu} \begin{pmatrix} \dfrac{4\hat{\alpha}_{\mathrm{s}}^2 K_1 r^{1+\lambda_1}}{(1+\lambda_1)\sin(-\pi\lambda_1)} \\ \dfrac{-(\hat{\alpha}_{\mathrm{s}}^2-1)^2 K_2 r^{1+\lambda_2}}{(1+\lambda_2)\sin(-\pi\lambda_2)} \end{pmatrix}. \tag{5.18}$$

(*b*) *Solid I is elastic, but solid II is rigid*

This case was considered by Liu *et al*. (1995). For a rigid solid, $\boldsymbol{B}_{\mathrm{II}} = \boldsymbol{0}$, so that $\boldsymbol{H} = \boldsymbol{B}_{\mathrm{I}}$, and it is given by (5.9) for the crack speed between the two sonic speeds of solid I, $c_{\mathrm{s}} < v < c_{\mathrm{l}}$. The real and imaginary parts of $\boldsymbol{H}$ are

$$\boldsymbol{M} = \frac{\alpha_{\mathrm{l}}(\hat{\alpha}_{\mathrm{s}}^2+1)}{[16\hat{\alpha}_{\mathrm{s}}^2\alpha_{\mathrm{l}}^2+(\hat{\alpha}_{\mathrm{s}}^2-1)^4]\mu}\begin{bmatrix} 4\hat{\alpha}_{\mathrm{s}}^2 & 2\hat{\alpha}_{\mathrm{s}}(\hat{\alpha}_{\mathrm{s}}^2-1) \\ -2\hat{\alpha}_{\mathrm{s}}(\hat{\alpha}_{\mathrm{s}}^2-1) & -(\hat{\alpha}_{\mathrm{s}}^2-1)^2 \end{bmatrix}, \tag{5.19}$$

$$\boldsymbol{N} = \frac{1}{[16\hat{\alpha}_{\mathrm{s}}^2\alpha_{\mathrm{l}}^2+(\hat{\alpha}_{\mathrm{s}}^2-1)^4]\mu}\begin{bmatrix} \hat{\alpha}_{\mathrm{s}}(\hat{\alpha}_{\mathrm{s}}^2-1)^2(\hat{\alpha}_{\mathrm{s}}^2+1) & (\hat{\alpha}_{\mathrm{s}}^2-1)^3-8\hat{\alpha}_{\mathrm{s}}^2\alpha_{\mathrm{l}}^2 \\ -(\hat{\alpha}_{\mathrm{s}}^2-1)^3+8\hat{\alpha}_{\mathrm{s}}^2\alpha_{\mathrm{l}}^2 & 4\hat{\alpha}_{\mathrm{s}}\alpha_{\mathrm{l}}^2(\hat{\alpha}_{\mathrm{s}}^2+1) \end{bmatrix}. \tag{5.20}$$

The eigenvalue problem (4.10) gives that

$$\lambda_1 = \frac{1}{\pi}\tan^{-1}\frac{\hat{\alpha}_{\mathrm{s}}\alpha_{\mathrm{l}}[(\hat{\alpha}_{\mathrm{s}}^2-1)^2-4]}{(\hat{\alpha}_{\mathrm{s}}^2-1)^2+4\hat{\alpha}_{\mathrm{s}}^2\alpha_{\mathrm{l}}^2}, \qquad \boldsymbol{w}_1 = \frac{1}{\sqrt{1+\hat{\alpha}_{\mathrm{s}}^2}}\begin{pmatrix} -1 \\ \hat{\alpha}_{\mathrm{s}} \end{pmatrix}, \tag{5.21 a}$$

$$\lambda_2 = 0, \qquad \boldsymbol{w}_2 = \frac{1}{1+\hat{\alpha}_{\mathrm{s}}^2}\begin{pmatrix} 1-\hat{\alpha}_{\mathrm{s}}^2 \\ 2\hat{\alpha}_{\mathrm{s}} \end{pmatrix}. \tag{5.21 b}$$

Because the λ_2 mode is non-singular, we will focus on the λ_1 mode. Corresponding to this mode, the tractions a distance r ahead of the crack tip are

$$\sigma_{21} = \frac{-K_1 r^{\lambda_1}}{\sqrt{1+\hat{\alpha}_{\mathrm{s}}^2}}, \qquad \sigma_{22} = \frac{\hat{\alpha}_{\mathrm{s}}K_1 r^{\lambda_1}}{\sqrt{1+\hat{\alpha}_{\mathrm{s}}^2}} \tag{5.22}$$

and the displacement jumps a distance r behind the crack tip are

$$\begin{bmatrix} d_1 \\ d_2 \end{bmatrix} = \frac{\hat{\alpha}_{\mathrm{s}}\alpha_{\mathrm{l}}(3-\hat{\alpha}_{\mathrm{s}}^2)\sqrt{1+\hat{\alpha}_{\mathrm{s}}^2}}{16\hat{\alpha}_{\mathrm{s}}^2\alpha_{\mathrm{l}}^2+(\hat{\alpha}_{\mathrm{s}}^2-1)^4}\frac{K_1 r^{1+\lambda_1}}{(1+\lambda_2)\sin(-\pi\lambda_1)\mu}\begin{pmatrix} -2\hat{\alpha}_{\mathrm{s}} \\ \hat{\alpha}_{\mathrm{s}}^2-1 \end{pmatrix}. \tag{5.23}$$

This mode has both shear and normal stress components on the interface.

6. Cohesive zone model

In the above, the crack tip is idealized as a structureless point, so that the stress field is singular. For a static or subsonic crack, this singularity is circumvented by an energetic consideration. Irwin (1957) showed that the mechanical free energy reduction associated with a crack advancing per unit area is given by

$$\mathcal{G} = \frac{1}{2\Delta}\int_0^{\Delta} \boldsymbol{t}^{\mathrm{T}}(\Delta - r)\boldsymbol{d}(r)\,\mathrm{d}r, \tag{6.1}$$

where Δ is an arbitrary length-scale. The traction $\boldsymbol{t}$ and displacement jump $\boldsymbol{d}$ are given by (4.16) and (4.17), respectively. For a subsonic crack, the matrix $\boldsymbol{H}$ is Hermitian, and the structure of the eigenvalue problem (4.10) is such that $\mathcal{G}$ is independent of the choice of Δ (Ting 1986; Bassani & Qu 1989; Suo 1990; Yang *et al*. 1991). In fracture mechanics, $\mathcal{G}$ is compared with the surface energy or a generalization of it to determine whether a crack will grow.

For an intersonic crack, however, the matrix $\boldsymbol{H}$ is no longer Hermitian. Consequently, $\mathcal{G}$ calculated according to (4.16), (4.17) and (6.1) depends on the choice of Δ. If we follow Irwin's original treatment to allow $\Delta \to 0$, then $\mathcal{G}$ is either zero or

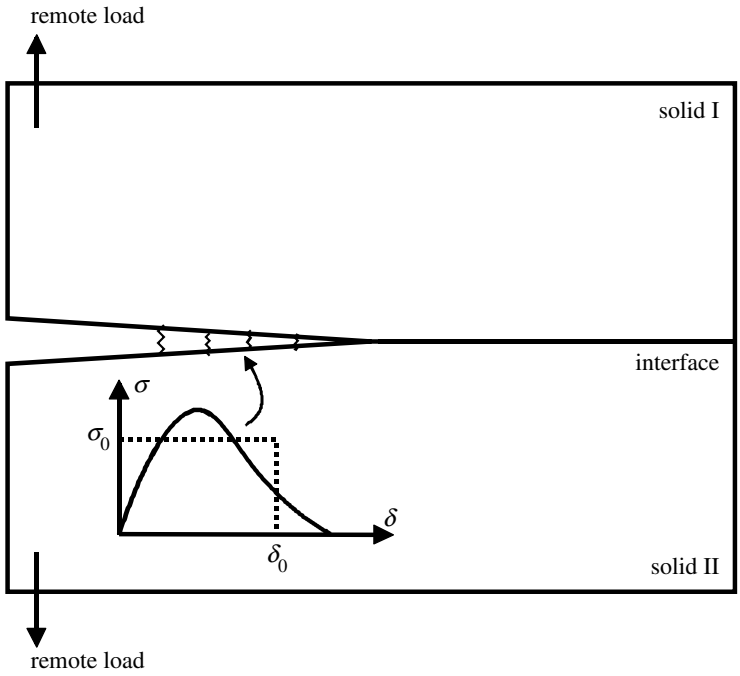

Figure 3. Cohesive zone model.

infinite. Consequently, this model cannot determine whether the crack can propagate at any given speed. (One may, of course, choose a finite Δ in the definition of $\mathcal{G}$. We will not pursue the matter along this line in this paper.)

To resolve the difficulty, we will abandon the idealization of the structureless crack tip, and invoke a model equipped with some description of the debonding process. One of the simplest such models, the cohesive zone model, will be analysed in this section. The model was introduced by Barenblatt (1962) for static cracks, and extended by various investigators for subsonic cracks (see, for example, Dmowska & Rice 1986; Freund 1990). We now explore the implications of this model for intersonic cracks.

Figure 3 illustrates the cohesive zone model. When loads are applied on the external boundary, the bonds at the interface supply tractions to resist fracture. Instead of a mathematical point, the 'crack tip' is now described by a zone of finite length, in which the bonds are characterized by a traction-separation law, $\sigma(\delta)$. This law must be nonlinear, because the traction vanishes for both small and large separations. For some calculations below, we will use the Dugdale (1960) rectilinear law (the dashed line in the inset of figure 3). Thus, the bonds are characterized by two quantities: strength σ_0 and the limiting separation δ_0. Two types of bimaterials discussed in § 5 will be treated. For an interface between a pair of weakly joined identical solids, we will separately consider the opening mode and the shear mode. For an interface between an elastic and a rigid solid, we will consider the mode with a real non-vanishing singularity exponent.

Thus, in general, we consider an arbitrary mode specified by a real-valued singularity exponent λ and a real-valued eigenvector $\boldsymbol{w}$. Coupled modes with complex singularity exponents will not be treated. Figure 4 shows the model as a superposition

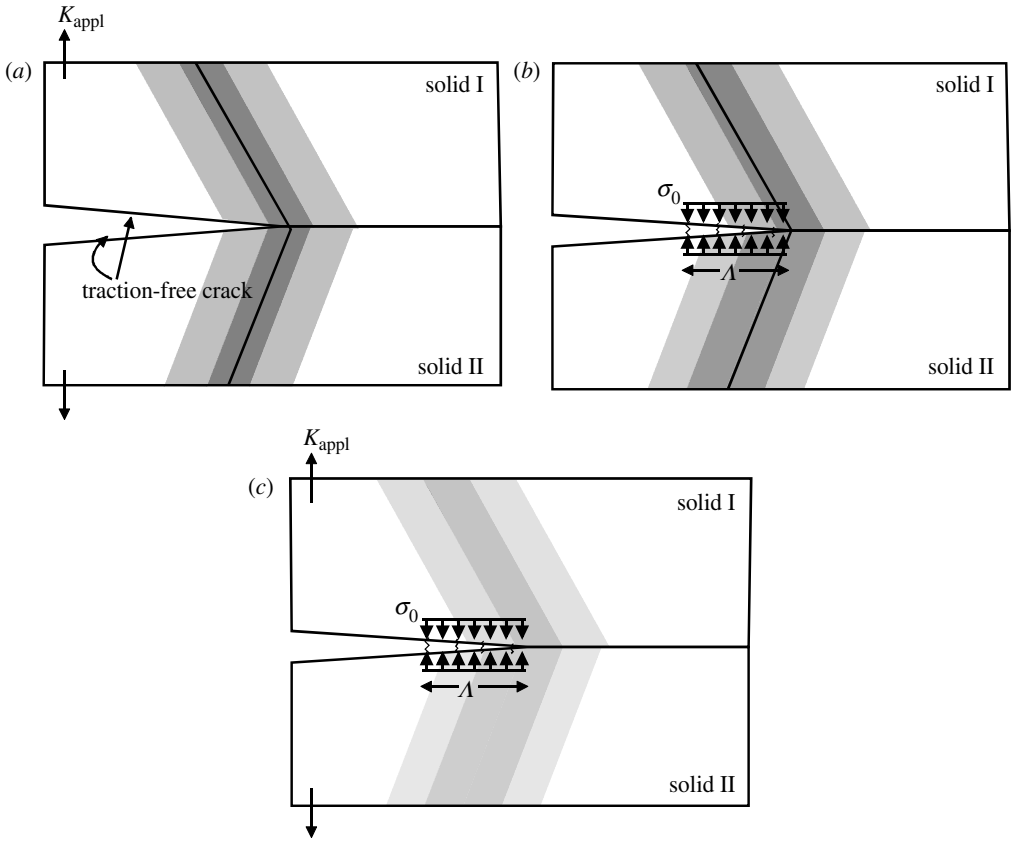

Figure 4. (a) Singular fields produced by the remote load without the distributed interfacial traction. The singularity exists along the two solid lines emanating from the crack tip. The shaded bands represent an intense deformation field. (b) Singular fields produced by the distributed interfacial traction. (c) Superposition of (a) and (b). The singularity is eliminated. The deformation field is still intense in the shaded bands, of a width scaling with the cohesive zone size Λ.

of two fields. Figure 4a illustrates the asymptotic field determined in § 4. Without the cohesive traction, the stress field caused by the remote load is singular not only at the crack tip but also along the two Mach lines emanating from the tip. According to (4.11), this field is represented by

$$\boldsymbol{h}(\zeta) = \frac{K_{\text{appl}}\zeta^{\lambda}\boldsymbol{w}}{1-\exp(2\pi \mathrm{i}\lambda)}. \tag{6.2}$$

The magnitude of the stress intensity factor K_{appl} will be determined shortly.

Figure 4b shows the field due to the interfacial bonds. The bonds supply a distributed traction vector on the crack surface, in the direction $\boldsymbol{w}$:

$$\boldsymbol{t}(x) = \sigma_0(x)\boldsymbol{w}, \quad x < 0. \tag{6.3}$$

The solution for the inhomogeneous Riemann–Hilbert problem (4.6) with this pre-

scribed traction is (Muskhelishvili 1953)

$$\boldsymbol{h}(\zeta) = \frac{\zeta^{\lambda}\boldsymbol{w}}{2\pi \mathrm{i}\exp(\pi \mathrm{i}\lambda)} \int_{-\infty}^{0} \frac{\sigma_0(x)\,\mathrm{d}x}{(-x)^{\lambda}(x-\zeta)}. \tag{6.4}$$

As $\zeta \to 0$, the function approaches to

$$\boldsymbol{h}(\zeta) = -\frac{\zeta^{\lambda}\boldsymbol{w}}{2\pi \mathrm{i}\exp(\pi \mathrm{i}\lambda)} \int_{-\infty}^{0} \frac{\sigma_0(x)\,\mathrm{d}x}{(-x)^{\lambda+1}}. \tag{6.5}$$

Consequently, the interfacial traction also induces a $\zeta^{\lambda}\boldsymbol{w}$ singularity.

The net field is the superposition of that due to the remote load (figure 4*a*) and that due to the interfacial traction (figure 4*b*). The sum of (6.2) and (6.4) is bounded as $\zeta \to 0$ provided the K_{appl} relates to σ_0 as

$$K_{\mathrm{appl}} = \frac{\sin(-\pi\lambda)}{\pi} \int_{-\infty}^{0} \frac{\sigma_0(x)\,\mathrm{d}x}{(-x)^{1+\lambda}}. \tag{6.6}$$

A superposition of the field (6.2) and (6.4) gives the total field:

$$\boldsymbol{h}(\zeta) = \frac{\zeta^{1+\lambda}\boldsymbol{w}}{2\pi \mathrm{i}\exp(\pi \mathrm{i}\lambda)} \int_{-\infty}^{0} \frac{\sigma_0(x)\,\mathrm{d}x}{(-x)^{1+\lambda}(\zeta-x)}. \tag{6.7}$$

As illustrated in figure 4*c*, the superimposed field is bonded, and is intense in bands of a finite width.

The displacement jump can be calculated by combining (4.7) and (6.7), giving

$$\boldsymbol{d}(r) = \frac{\boldsymbol{M}\boldsymbol{w}}{\pi} \int_{0}^{r} \mathrm{d}\xi \int_{-\infty}^{0} \mathrm{d}x \left(\frac{\xi}{-x}\right)^{1+\lambda} \frac{\sigma_0(x)}{x+\xi}. \tag{6.8}$$

For a mode with the interfacial traction in the $\boldsymbol{w}$-direction, the displacement jump is in the $\boldsymbol{M}\boldsymbol{w}$-direction. The two directions coincide for either mode for an interface between a pair of identical solids, but differ for an interface between an elastic and a rigid solid.

Let Λ be the cohesive zone length (figure 4*b*), namely, the interfacial traction vanishes at the tail of the cohesive zone, $x = -\Lambda$. To be consistent with the small-scale yielding and small-scale contact assumption, the cohesive zone size, Λ, is taken to be small compared with the crack length and other lengths that describe the macroscopic sample. Using the rectilinear law, we obtain from (6.8) the separation at the tail of the cohesive zone:

$$\boldsymbol{d}(\Lambda) = \frac{\sigma_0 \Lambda Q}{\pi} \boldsymbol{M}\boldsymbol{w}. \tag{6.9}$$

The dimensionless factor

$$Q = \int_{0}^{1}\int_{0}^{1} \left(\frac{\xi}{x}\right)^{\lambda+1} \frac{\mathrm{d}\xi\,\mathrm{d}x}{\xi - x} \tag{6.10}$$

can be calculated numerically. Note that Q depends only on λ and $Q > 0$ for $-1 < \lambda < 0$. Equating $\boldsymbol{w}^{\mathrm{T}} \cdot \boldsymbol{d}(\Lambda)$ to the limiting separation δ_0, we find the cohesive zone length:

$$\Lambda = \frac{\pi\delta_0}{\sigma_0 Q \boldsymbol{w}^{\mathrm{T}}\boldsymbol{M}\boldsymbol{w}}. \tag{6.11}$$

The interfacial parameters σ_0 and δ_0 are taken to be independent of the crack speed in this model. The length Λ will vary with the crack speed because of the other factors in (6.11).

For a static opening crack in a homogeneous solid, the cohesive zone length is

$$\Lambda_0 = \frac{\pi\mu\delta_0}{4(1-\nu)\sigma_0}. \tag{6.12}$$

We will use Λ_0 to normalize the cohesive zone length for other cases:

$$\frac{\Lambda}{\Lambda_0} = \frac{4(1-\nu)}{\mu \boldsymbol{w}^{\mathrm{T}} \boldsymbol{M} \boldsymbol{w} Q}. \tag{6.13}$$

We will examine this result in some detail as follows. Poisson's ratio will be set as $\nu = \frac{1}{3}$, so that Λ/Λ_0 is only a function of the normalized crack speed v/c_{s}.

(*a*) *Solid I and II are identical*

For this limiting case, when the crack speed is subsonic, the cohesive zone length is

$$\frac{\Lambda}{\Lambda_0} = \frac{(1-\nu)[4\alpha_{\mathrm{l}}\alpha_{\mathrm{s}} - (1+\alpha_{\mathrm{s}}^2)^2]}{(1-\alpha_{\mathrm{s}}^2)} \begin{cases} 1/\alpha_{\mathrm{l}}, & \text{opening mode,} \\ 1/\alpha_{\mathrm{s}}, & \text{shear mode.} \end{cases} \tag{6.14}$$

When the crack speed is intersonic, the cohesive zone length is

$$\frac{\Lambda}{\Lambda_0} = \frac{4(1-\nu)[16\hat{\alpha}_{\mathrm{s}}^2\alpha_{\mathrm{l}}^2 + (\hat{\alpha}_{\mathrm{s}}^2-1)^4]}{Q\alpha_{\mathrm{l}}(\hat{\alpha}_{\mathrm{s}}^2+1)} \begin{cases} -\dfrac{1}{(\hat{\alpha}_{\mathrm{s}}^2-1)^2}, & \text{opening mode,} \\ \dfrac{1}{4\hat{\alpha}_{\mathrm{s}}^2}, & \text{shear mode.} \end{cases} \tag{6.15}$$

Figure 5 plots the length of the cohesive zone as a function of the crack speed for the opening mode. The cohesive zone size becomes negative when $v > c_{\mathrm{R}}$. It is seen from (6.11) that the sign of Λ is determined by the sign of $\boldsymbol{w}^{\mathrm{T}}\boldsymbol{M}\boldsymbol{w}$. Its physical significance may be understood as follows. The interfacial traction is in the direction $\boldsymbol{w}$, equation (6.3), and the displacement jump is in direction $\boldsymbol{M}\boldsymbol{w}$, equation (6.8). For the interfacial traction to do work to resist debonding, the inner product of the two vectors, $\boldsymbol{w}^{\mathrm{T}}\boldsymbol{M}\boldsymbol{w}$, must be positive. Consequently, within this model, $\Lambda < 0$ is equivalent to the inability of the interfacial bonds to do work to resist debonding. We take this as the condition that the crack cannot propagate. Thus the opening mode intersonic crack is not permitted by the model.

For the shear crack (figure 6), the cohesive zone size is negative when $c_{\mathrm{R}} < v < c_{\mathrm{s}}$ approaches infinity as $v \to c_{\mathrm{s}}$, and then becomes positive when $c_{\mathrm{s}} < v < c_{\mathrm{l}}$. This indicates that if the crack can cross the narrow speed region $c_{\mathrm{R}} < v < c_{\mathrm{s}}$, it can propagate intersonically. In a homogeneous solid, a shear crack tends to deviate from the original crack plane. It would be interesting, then, to carry out an experiment with two weakly joined solids, such as two glass slides joined by optical contact. The weak interface would confine the crack to the plane. If the above explanation is correct, such a crack will approach the Rayleigh wave speed. With some perturbation, the crack may even jump to an intersonic speed. We are unable to judge whether this process is realistic based on experimental information available to us.

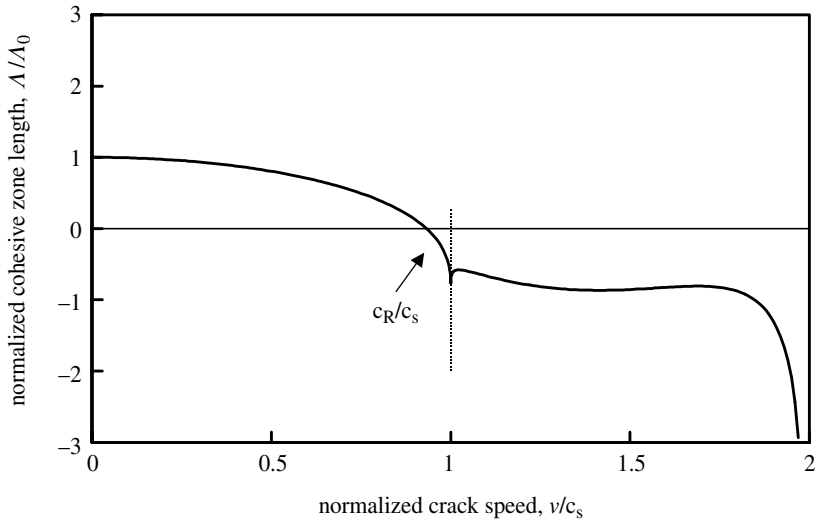

Figure 5. Cohesive zone length as a function of the crack speed for weakly joined identical solids (opening mode).

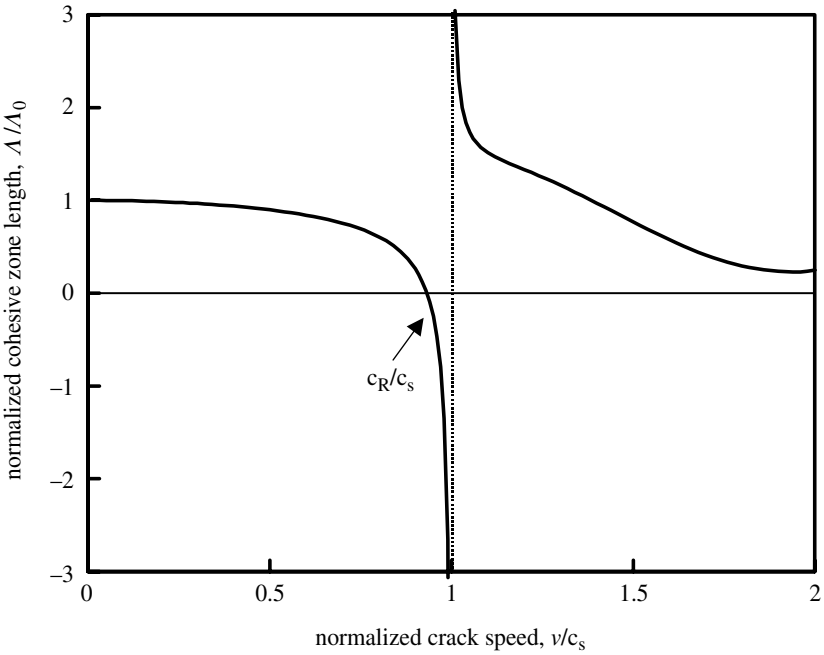

Figure 6. Cohesive zone length as a function of the crack speed for weakly joined identical solids (shear mode).

(*b*) *Solid I is elastic, but solid II is rigid*

In this case, we will only discuss the intersonic crack because the subsonic crack has a pair of complex-conjugate singularity exponents, which complicates the model.

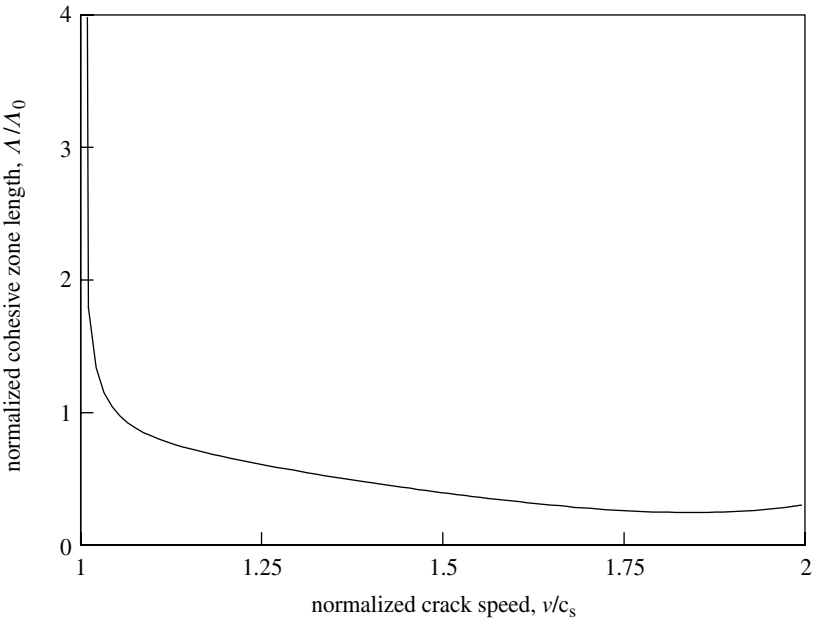

Figure 7. Cohesive zone length as a function of the crack speed for an intersonic crack on the interface between an elastic and a rigid solid.

The cohesive zone length is

$$\frac{\Lambda}{\Lambda_0} = \frac{4(1-\nu)[16\hat{\alpha}_s^2\alpha_l^2 + (\hat{\alpha}_s^2-1)^4]}{Q\hat{\alpha}_s^2\alpha_l(3-\hat{\alpha}_s^2)(1+\hat{\alpha}_s^2)}. \tag{6.16}$$

Figure 7 plots the cohesive zone length as a function of the normalized crack speed ($\nu = \frac{1}{3}$). Comparing figures 6 and 7, we note no qualitative difference between the shear mode intersonic crack on an interface of weakly joined identical solids, and the λ_1-mode intersonic crack on an elastic–rigid bimaterial interface. The latter case approximately represents the polymer–metal pairs used in the experiments of Rosakis and co-workers (Liu *et al*. 1993; Lambros & Rosakis 1995*a–c*; Singh *et al*. 1997), where crack speeds between the shear and the longitudinal wave speeds of the polymer have been recorded.

If $\nu > \frac{1}{3}$, $\lambda_1 \to 0$ when $v \to 2c_s$; if $\nu \leqslant \frac{1}{3}$, $\lambda_1 \to 0$ when $v \to c_l$. Consequently, at the large crack speeds, the a_{10} singularity in the Williams expansion is so weak that there no longer exists a region in which the r^{λ_1} term dominates. The current model cannot predict what happens at that stage. One has to use other terms in the Williams expansion, which should be investigated further.

7. Concluding remarks

The stress field around an intersonic crack is governed by a mixture of elliptic and hyperbolic differential equations. We introduce a unified method to analyse the stress field around a crack running uniformly on an interface. The crack speed can be static, subsonic or intersonic; the two solids can be isotropic or anisotropic. The full Williams-type expansion of the crack tip field is obtained. We then extend the

Barenblatt cohesive zone model to intersonic cracks. The model removes the singularity both at the crack tip and along the Mach line. A length-scale characterizes the size of the cohesive zone and the thickness of the shock front. This length depends on the crack speed. We postulate that a crack speed is forbidden if it results in a negative cohesive zone size. The predictions of the model qualitatively agree with the available experimental observations and suggest additional experiments. In particular, we find no qualitative difference between the shear mode intersonic crack for weakly joined identical solids and the λ_1-mode intersonic crack on an elastic–rigid bimaterial interface.

This work is supported by the National Science Foundation through grant CMS-9820713, and by The Institute for Materials Research and Engineering, Singapore.

Appendix A.

Here we establish the connection between the method used in this paper and that in Yu & Yang (1995). In the upper half-plane, no matter how large the crack speed is, we always have the representations (3.4) and (3.5):

$$\boldsymbol{u}_{\mathrm{I}}'(x) = \boldsymbol{A}_{\mathrm{I}}\boldsymbol{f}_{\mathrm{I}}'(x) + \bar{\boldsymbol{A}}_{\mathrm{I}}\bar{\boldsymbol{f}}_{\mathrm{I}}'(x), \tag{A 1}$$

$$\boldsymbol{t}(x) = \boldsymbol{L}_{\mathrm{I}}\boldsymbol{f}_{\mathrm{I}}'(x) + \bar{\boldsymbol{L}}_{\mathrm{I}}\bar{\boldsymbol{f}}_{\mathrm{I}}'(x). \tag{A 2}$$

Because $\boldsymbol{t}(x)$ is real, if $\boldsymbol{f}_{\mathrm{I}}'$ vanishes as $|\zeta| \to \infty$ and the singularity of $\boldsymbol{f}_{\mathrm{I}}'$ is weaker than ζ^{-1}, the Plemelj formulae requires that

$$\boldsymbol{L}_{\mathrm{I}}\boldsymbol{f}_{\mathrm{I}}'(\zeta) = \frac{1}{2\pi\mathrm{i}}\int_{-\infty}^{\infty}\frac{\boldsymbol{t}(\xi)}{\xi-\zeta}\,\mathrm{d}\xi, \quad \zeta \in \mathrm{I}. \tag{A 3}$$

As ζ approaches the x-axis,

$$\boldsymbol{L}_{\mathrm{I}}\boldsymbol{f}_{\mathrm{I}}'^{+}(x) = \tfrac{1}{2}t(x) + \frac{1}{2\pi\mathrm{i}}\int_{-\infty}^{\infty}\frac{\boldsymbol{t}(\xi)}{\xi-x}\,\mathrm{d}\xi. \tag{A 4}$$

A substitution of (A 4) into (A 1) relates the displacement and the traction on the x-axis:

$$\boldsymbol{u}_{\mathrm{I}}'(x) = \mathrm{Im}(\boldsymbol{B}_{\mathrm{I}})\boldsymbol{t}(x) - \frac{\mathrm{Re}(\boldsymbol{B}_{\mathrm{I}})}{\pi}\int_{-\infty}^{\infty}\frac{\boldsymbol{t}(\xi)}{\xi-x}\,\mathrm{d}\xi. \tag{A 5}$$

Similarly, in the lower half-plane, one has

$$\boldsymbol{L}_{\mathrm{II}}\boldsymbol{f}_{\mathrm{II}}'(\zeta) = -\frac{1}{2\pi\mathrm{i}}\int_{-\infty}^{\infty}\frac{\boldsymbol{t}(\xi)}{\xi-\zeta}\,\mathrm{d}\xi, \quad \zeta \in \mathrm{II}. \tag{A 6}$$

The relation between the displacement and the traction is

$$\boldsymbol{u}_{\mathrm{II}}'(x) = \mathrm{Im}(\boldsymbol{B}_{\mathrm{II}})\boldsymbol{t}(x) + \frac{\mathrm{Re}(\boldsymbol{B}_{\mathrm{II}})}{\pi}\int_{-\infty}^{\infty}\frac{\boldsymbol{t}(\xi)}{\xi-x}\,\mathrm{d}\xi. \tag{A 7}$$

References

Barenblatt, G. I. 1962 The mathematical theory of equilibrium cracks in brittle fracture. *Adv. Appl. Mech.* **7**, 55–129.

Barnett, D. M. & Lothe, J. 1985 Free surface (Rayleigh) waves in anisotropic elastic half-spaces: the surface impedance method. *Proc. R. Soc. Lond.* A **402**, 135–152.

Bassani, J. L. & Qu, J. 1989 Finite crack on bimaterial and bicrystal interfaces. *J. Mech. Phys. Solids* **37**, 434–453.

Dmowska, R. & Rice, J. R. 1986 Fracture theory and its seismological applications. In *Continuum theories in solid Earth physics* (ed. R. Teisseyre). Physics and Evolution of the Earth's Interior, vol. 3, pp. 187–255. Elsevier.

Dugdale, D. C. 1960 Yielding of steel sheets containing slits. *J. Mech. Phys. Solids* **8**, 100–104.

Freund, L. B. 1990 *Dynamic fracture mechanics*. Cambridge University Press.

Gao, H. 1993 Surface roughening and branching instabilities in dynamic fracture. *J. Mech. Phys. Solids* **41**, 457–486.

Hui, C. Y. & Ruina, A. 1995 Why K? High order singularities and small scale yielding. *Int. J. Fracture* **72**, 97–120.

Irwin, G. R. 1957 Analysis of stresses and strains near the end of a crack traversing a plate. *J. Appl. Mech.* **24**, 361–364.

Lambros, J. & Rosakis, A. J. 1995*a* Dynamic decohesion of bimaterials: experimental observations and failure criteria. *Int. J. Solids Struct.* **32**, 2677–2702.

Lambros, J. & Rosakis, A. J. 1995*b* Shear dominated transonic interfacial crack growth in a bimaterial. I. Experimental observations. *J. Mech. Phys. Solids* **43**, 169–188.

Lambros, J. & Rosakis, A. J. 1995*c* Development of a dynamic decohesion criterion for subsonic fracture of the interface between two dissimilar materials. *Proc. R. Soc. Lond.* A **451**, 711–736.

Liu, C., Lambros, J. & Rosakis, A. J. 1993 Highly transient elastodynamic crack growth in a bimaterial interface: higher order asymptotic analysis and experiments. *J. Mech. Phys. Solids* **41**, 1887–1954.

Liu, C., Huang, Y. & Rosakis, A. J. 1995 Shear dominated transonic interfacial crack growth in a bimaterial. II. Asymptotic fields and favorable velocity regimes. *J. Mech. Phys. Solids* **43**, 189–206.

Muskhelishvili, N. I. 1953 *Singular integral equations*. Gröningen: Noordhoff.

Rice, J. R. 1988 Elastic fracture mechanics concepts for interfacial cracks. *J. Appl. Mech.* **110**, 98–103.

Singh, R. P., Lambros, J. Shukla, A. & Rosakis, A. J. 1997 Investigation of the mechanics of intersonic crack propagation along a bimaterial interface using coherent gradient sensing and photoelasticity. *Proc. R. Soc. Lond.* A **453**, 2649–2667.

Stroh, A. N. 1962 Steady state problems in anisotropic elasticity. *Math. Phys.* **41**, 77–103.

Suo, Z. 1990 Singularities, interfaces and cracks in dissimilar anisotropic media. *Proc. R. Soc. Lond.* A **427**, 331–357.

Ting, T. C. T. 1986 Explicit solution and invariance of the singularities at an interface crack in anisotropic composites. *Int. J. Solids Struct.* **22**, 965–983.

Washabaugh, P. D. & Knauss, W. G. 1994 A reconciliation of dynamic crack velocity and Rayleigh wave speed in isotropic brittle solids. *Int. J. Fracture* **65**, 97–114.

Williams, M. L. 1959 The stress around a fault or crack in dissimilar media. *Bull. Seismol. Soc. Am.* **49**, 199–204.

Willis, J. R. 1971 Fracture mechanics of interfacial cracks. *J. Mech. Phys. Solids* **19**, 353–368.

Wu, K. C. 1991 Explicit crack-tip fields of an extending interface crack in an anisotropic bimaterial. *Int. J. Solids Struct.* **27**, 455–466.

Yang, W., Suo, Z. & Shih, C. F. 1991 Mechanics of dynamic debonding. *Proc. R. Soc. Lond.* A **433**, 679–697.

Yu, H. H. & Yang, W. 1994 Mechanics of transonic debonding of a bimaterial interface: the anti-plane shear case. *J. Mech. Phys. Solids* **42**, 1789–1801.

Yu, H. H. & Yang, W. 1995 Mechanics of transonic debonding of a bimaterial interface: the in-plane case. *J. Mech. Phys. Solids* **43**, 207–232.